Topics in Catalysis (2018) 61:71–80
https://doi.org/10.1007/s11244-017-0875-0

ORIGINAL PAPER

Photoelectron Velocity Map Imaging Spectroscopy of Heteronuclear Metal–Nickel Carbonyls $M\mathrm{Ni(CO)}_n^-$ ($M = \mathrm{Sc, Y}$; $n = 2–6$)

Hua Xie[1] · **Jinghan Zou**[1,2] · **Qinqin Yuan**[1,2] · **Jumei Zhang**[1,2] · **Hongjun Fan**[1] · **Ling Jiang**[1]

Published online: 20 November 2017
© Springer Science+Business Media, LLC, part of Springer Nature 2017

Abstract

The chemical bonding and electronic structure of heteronuclear metal–nickel carbonyls $M\mathrm{Ni(CO)}_n^-$ ($M = \mathrm{Sc, Y}$; $n = 2–6$) have been investigated by mass-selected photoelectron velocity map imaging spectroscopy and quantum chemical calculations. Two CO bonding modes (side-on-bonded and terminal carbonyls) are involved in the $n = 2$ cluster. The building block composed of three kinds of different CO modes (side-on-bonded, bridging, and terminal carbonyls) is favored at $n = 3$, the structure of which persists up to $n = 6$. The additional CO ligands are preferentially coordinated in the terminal mode to the Sc atom and then to the Ni atom in the larger clusters. The present findings would promote the understanding of CO molecule activation and chemisorbed CO molecules on metal surfaces.

Keywords Photoelectron spectroscopy · CO activation · Heteronuclear metal carbonyl · Quantum chemical calculation

1 Introduction

Transition metal (TM) carbonyls have provided prototypical models of CO chemisorption on metal surface or the binding at active sites of catalyst, and shed light on the metal–ligand bonding in inorganic, organometallic, and coordination chemistry [1–3]. To date, an abundance of theoretical and experimental studies have been carried out on the spectroscopic and structural properties of these complexes. Experimentally, a series of the reactions of metals with CO molecules have been well characterized by mass spectrometry and the spectroscopic information of many metal–CO complexes have been measured by various kinds of spectroscopic technologies. The bonding energies of TM carbonyls were measured using collision-induced dissociation [4–6]. Matrix-isolation infrared spectroscopy has been employed to study various charged and neutral metal carbonyls in both rare gas matrices and condensed phase environments [7–10]. Infrared photodissociation (IRPD) spectroscopy combined with theoretical calculations has been successfully applied to probe the structures and vibrational frequencies of the homoleptic mononuclear and multinuclear TM carbonyl clusters [11–16]. Equilibrium geometries and vibrational frequencies of TM carbonyl clusters have been established from the Fourier-transform microwave spectroscopy [17]. Photoelectron spectroscopy (PES) has been used to investigate mass-selected TM carbonyl anions and revealed much information about their electronic structures [18–21]. Theoretically, much effort has been devoted to TM carbonyls, with the aim of obtaining the unusual features of the metal–metal and metal–carbon bonds and supporting the experimental observed intriguing properties. Both density functional theory (DFT) and ab initio quantum chemical methods have been used to examine plausible structures for the mononuclear and dinuclear TM carbonyls [22–25].

Binuclear metal carbonyls have gained extensive interest in various kinds of experimental and theoretical observations. Recently, the studies of homo-binuclear metal carbonyls have mainly focused on the reaction of CO molecule with metal clusters in the gas phase. A series of binuclear monocarbonyl clusters, such as $\mathrm{Sc_2CO}$, $\mathrm{Mn_2CO}$, $\mathrm{Fe_2CO}$,

---

Electronic supplementary material The online version of this article (https://doi.org/10.1007/s11244-017-0875-0) contains supplementary material, which is available to authorized users.

✉ Ling Jiang
ljiang@dicp.ac.cn

[1] State Key Laboratory of Molecular Reaction Dynamics, Collaborative Innovation Center of Chemistry for Energy and Materials (iChEM), Dalian Institute of Chemical Physics, Chinese Academy of Sciences, 457 Zhongshan Road, Dalian 116023, Liaoning, China

[2] University of Chinese Academy of Sciences, 19A Yuquan Road, Beijing 100049, China

Co_2CO et al., have been investigated to probe the interaction and behavior between CO molecule with the metals using infrared spectroscopy [7, 26–30]. Theoretical studies also revealed different bonding modes (side-on-bonded, bridging, and terminal carbonyls) of single CO to the binuclear 3d metals [22, 23, 31]. For larger clusters, IRPD studies have found that the $Cr_2(CO)_n^+$ ($n=7$–9) cluster cations possess the $(OC)_5Cr–C–O–Cr(CO)_{n-6}^+$ structures with a linear bridging carbonyl group bonded to one Cr atom through its carbon atom and to the other Cr atom through its oxygen atom [16]. The $Fe_2(CO)_n^-$ ($n=4$–7) cluster anions have unusual asymmetric $(OC)_4Fe––Fe(CO)_{n-4}^-$ structures [14]. The $Co_2(CO)_8^+$ cation was determined to be a Co–Co bonded structure with C_s symmetry involving a bridging CO ligand and the $Co_2(CO)_9^+$ cation has a mixture of the CO-tagged $Co_2(CO)_8^+$–CO complex and the $Co(CO)_5^+$–$Co(CO)_4$ ion-molecular complex [32]. The $Cu_2(CO)_6^+$ cation has the $(OC)_3Cu–Cu(CO)_3^+$ structure and the $Cu_2(CO)_7^+$ cation was determined to be a weakly bound complex involving a $Cu_2(CO)_6^+$ core ion [33]. Additionally, PES investigations have indicated that $Au_2(CO)$ and $Au_2(CO)_2^{-/0}$ were found to be linear molecules with CO coordinated to Au terminally via C, and $Au_2(CO)^-$ is revealed to be bent. $Au_2(CO)_3^{-/0}$ were found to be physisorbed complexes, in which the third CO is weakly interacting with a linear $Au_2(CO)_2^-$ core [34]. In the $Ti_2(CO)_n^-$ ($n=4$–6) series, $Ti_2(CO)_4^-$ consists of three side-on-bonded CO molecules and one terminally bonded CO molecule, and $Ti_2(CO)_5^-$ is derived from $Ti_2(CO)_4^-$ by bonding terminally the fifth CO to the Ti atom; $Ti_2(CO)_6^-$ has two side-on-bonded CO molecules and four terminal CO molecules [35].

In contrast, few efforts have been involved for heterobinuclear metal carbonyls. IRPD spectroscopic studies have revealed that the $MFe(CO)_8^+$ ($M=$ Co, Ni, Cu) complexes have eclipsed $(CO)_5Fe–M(CO)_3^+$ structures and $MCu(CO)_7^+$ ($M=$ Co, Ni) have staggered $(CO)_4M–Cu(CO)_3^+$ structures, the $FeZn(CO)_5^+$ complex has a $(CO)_5Fe–Zn^+$ structure and the $CoZn(CO)_7^+$ ion has a $(CO)_4Co–Zn(CO)_3^+$ structure [36, 37]. PES investigations of $MNi(CO)_3^-$ ($M=$ Mg, Ca, Al, Cu) have indicated that the three carbonyls are bonded terminally to the Ni atom, resulting in the formation of the $Ni(CO)_3$ motif [38, 39]. In the $PbFe(CO)_4^-$ clusters, the four carbonyls are bonded terminally to the Fe atom [40]. In these heterobinuclear metal carbonyls mentioned above, the main metal–CO coordination mode is terminal. Recently, PES spectroscopy of $MNi(CO)_n^-$ ($M=$ Ti, Zr, Hf; $n=3$–7) has revealed that three different kinds of CO bonding configurations are successfully captured in the $n=3$ cluster and the building block of three bridging CO molecules ($TiNi(\mu\text{-}CO)_3$) is favored at $n=4$, which is retained up to $n=7$ [41].

The MNi ($M=$ Sc, Y) heterobimetals are widely involved in many catalytic processes [42–44]. Nickel tetracarbonyl was the first metal carbonyl to be prepared in 1890, and nickel group carbonyls are among the most studied metal carbonyls both experimentally and theoretically [45]. In the present work, we report a study on a series of heteronuclear metal-nickel clusters $MNi(CO)_n^-$ ($M=$ Sc, Y; $n=2$–6). Photoelectron velocity-map imaging spectroscopic and theoretical investigations reveal that two CO bonding modes (side-on-bonded and terminal carbonyls) are involved in the $n=2$ cluster. The building block composed of three kinds of different CO modes (side-on-bonded, bridging, and terminal carbonyls) is favored at $n=3$, the structure of which persists up to $n=6$. The additional CO ligands are preferentially coordinated in the terminal mode to the Sc atom and then to the Ni atom in the larger clusters.

2 Experimental and Theoretical Methods

The experiments were performed using a homemade instrument with a laser vaporization source, a dual-channel time-of-flight mass spectrometer (D-TOFMS) coupled with velocity-map photoelectron imaging analyzer. Details of the apparatus have been described elsewhere [46], and only a brief outline is given below. The heterodinuclear transition metal carbonyl anions were generated by laser vaporization cluster source and these cluster anions were obtained in a supersonic expansion of helium gas seeded with 5% CO. The typical stagnation pressure of the carrier gas was about 1–5 atm. The cluster anions were cooled and expanded into the source chamber. The anions of interest were mass selected by a McLaren Wiley time-of-flight spectrometer and then introduced into the photodetachment region. The photon energy of 355 nm (3.496 eV) was used for the photodetachment of these anionic clusters. The resulting photoelectrons were extracted by a velocity map imaging photoelectron spectrometer and recorded by a charge-coupled device camera (CCD). Each image was obtained by accumulating 10,000–50,000 laser shots at 10 Hz repetition rate. The obtained raw image stood for the projection of the photoelectron density in the 3D laboratory frame onto the 2D imaging detector. The original 3D distribution was reconstructed using the Basis Set Expansion (BASEX) inverse Abel transform method, and the photoelectron spectrum was acquired. The photoelectron spectra were calibrated using the known spectrum of Au^-. The energy resolution was better than 5%, corresponding to 50 meV at electron kinetic energy (eKE) of 1 eV.

In order to explain the electronic and geometrical structures of $MNi(CO)_n^{0/-1}$ ($M=$ Sc, Y), theoretical calculations were performed using the Gaussian 09 programs [47]. Recent investigations have shown that the B3LYP function [48] works well for the scandium and yttrium carbonyls [49], and then was employed here. The Aug-cc-pVTZ basis set was selected for the C and O atoms [50], and the SDD (SC-RECP, MWB28) basis set for the Sc and Y atoms [51]. Harmonic frequency analysis was carried out to make sure that the obtained structures were real minima on the potential energy surfaces. The vertical detachment energy (VDE) was defined as the difference in energy between the neutral and anionic species based on the optimized anionic geometry, and the adiabatic detachment energy (ADE) was calculated as the difference in energy between the neutral and the anion both at their optimized geometries. Relative energies and the ADEs included the zero-point-energy corrections corrections. All possible spin states were considered. For the most stable isomers of $ScNi(CO)_n^-$, for example, the relative energies between singlet and triplet states are very close (Table S1). However, the calculated VDEs of the species with singlet states agree best with the experimental values. The calculated VDEs of the species with triplet states for the 4A, 5A, and 6A structures are much higher than the experimental values. Only the calculated results of the isomers with singlet states are shown for the present discussions.

3 Results and Analysis

3.1 Photoelectron Spectroscopy

The $M Ni(CO)_n^-$ ($M = Sc$, Y) complexes were produced via laser vaporization of metal rods with 5% CO seeded in helium. The mass spectrum of scandium-nickel and yttrium-nickel carbonyl cluster anions is given in Figs. S1 and S2 in the Supporting Information, respectively. Besides the $M Ni(CO)_n^-$ ($M = Sc$, Y; $n = 2$–6) target products, the $Ni(CO)_3^-$, $NiC(CO)_3^-$, $Fe(CO)_4^-$, $ScNiH_2O(CO)_n^-$ ($n = 3$–5), $ScNiC(CO)_n^-$ ($n = 3$–6), and $YNiO(CO)_n^-$ ($n = 1$–3) complexes were also observed. The carbonyl anions of interest were mass-selected and introduced into the photodetachment region. The photoelectron imaging results and corresponding photoelectron spectra of $M Ni(CO)_n^-$ ($M = Sc$, Y; $n = 2$–6) are shown in Figs. 1 and 2, respectively.

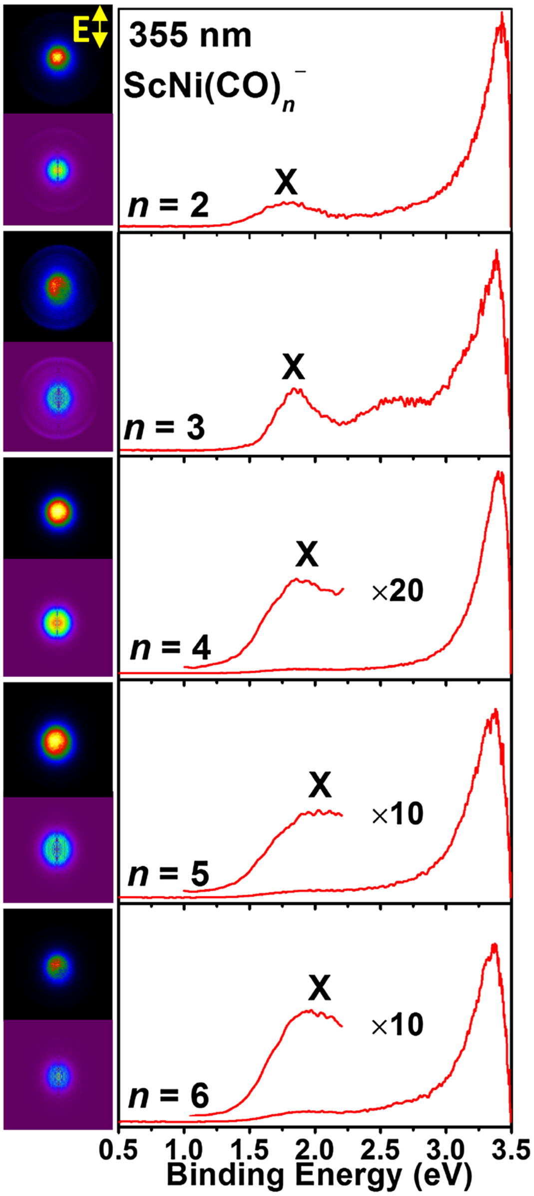

Fig. 1 Photoelectron images of $ScNi(CO)_n^-$ ($n = 2$–6) at 355 nm. The raw image (upper) and the reconstructed image (bottom) after inverse Abel transformation are shown on the left side. The double arrow indicates the direction of the laser polarization. Photoelectron spectra are shown on the right side

The single photon energy of 355 nm (3.496 eV) for $ScNi(CO)_n^-$ allows ground state transitions of all compounds to be observed, as shown in Fig. 1. The photoelectron spectra mainly reveal an intense X band, and the VDE values of $ScNi(CO)_n^-$ ($n = 2$–6) were estimated from their band maxima in the 355 nm spectra to be 1.76 ± 0.09, 1.83 ± 0.08, 1.86 ± 0.08, 1.94 ± 0.08, and 1.97 ± 0.08 eV (Table 1), respectively. The ADE value was estimated by drawing a straight line at the rising edge of the main band and then adding the instrumental resolution to the intersection with the binding energy axis. The ADE values of $ScNi(CO)_n^-$ ($n = 2$–6) were evaluated to be 1.53 ± 0.10, 1.68 ± 0.09, 1.70 ± 0.09, 1.73 ± 0.09, and 1.77 ± 0.09 eV (Table 1), respectively.

It can be seen from Fig. 2 that the 355 nm photoelectron images and spectra of $YNi(CO)_n^-$ ($n = 2$–6) are similar to those of $ScNi(CO)_n^-$. The VDE values of $YNi(CO)_n^-$ ($n = 2$–6) were estimated to be 1.70 ± 0.09, 1.89 ± 0.08, 1.96 ± 0.08, 2.12 ± 0.07, and 2.26 ± 0.06 eV (Table 2), respectively. The ADE values of $YNi(CO)_n^-$ ($n = 2$–6) were measured to be

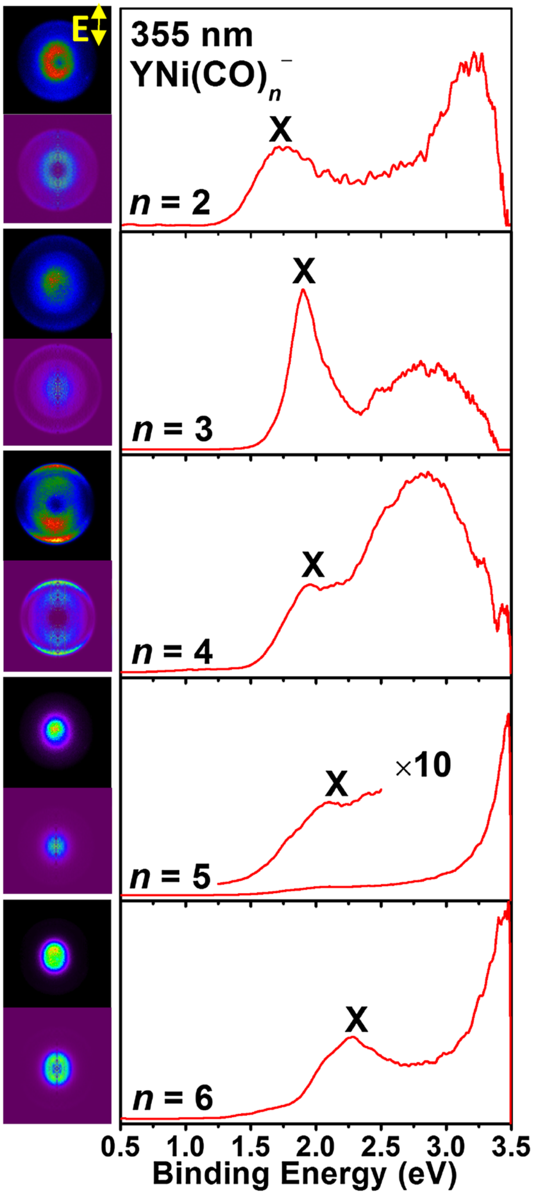

Fig. 2 Photoelectron images of YNi(CO)$_n^-$ (n=2–6) at 355 nm. The raw image (upper) and the reconstructed image (bottom) after inverse Abel transformation are shown on the left side. The double arrow indicates the direction of the laser polarization. Photoelectron spectra are shown on the right side

1.54 ± 0.10, 1.69 ± 0.09, 1.72 ± 0.09, 1.73 ± 0.09, and 1.77 ± 0.09 eV, respectively.

3.2 Comparison Between Experimental and Theoretical Results

Optimized structures of MNi(CO)$_n^-$ (M = Sc, Y; n = 2–6) are illustrated in Figs. 3 and 4, respectively. None of the triplet anions were found to be energetically competitive with the corresponding singlet isomers. Accordingly, only the results obtained for the representative low-energy isomers with the singlet electronic state are shown. Tables 1 and 2 list the comparison of experimental VDE and ADE values to B3LYP calculated ones of the four lowest-energy isomers for for MNi(CO)$_n^-$ (M = Sc, Y; n = 2–6), respectively.

Table 1 Comparison of experimental VDE and ADE values to the calculated ones of the four lowest-energy isomers for ScNi(CO)$_n^-$ (n=2–6)

Cluster	Isomer	VDE (eV)		ADE (eV)	
		Exp.[a]	Calc.	Exp.[a]	Calc.
n=2	2A	1.76 (9)	1.59	1.53 (10)	1.37
	2B		1.07		1.03
	2C		1.06		0.99
	2D		0.91		0.81
n=3	3A	1.83 (8)	1.65	1.68 (9)	1.55
	3B		1.20		1.10
	3C		1.22		1.05
	3D		1.18		1.09
n=4	4A	1.86(8)	1.76	1.70 (9)	1.60
	4B		1.49		1.37
	4C		1.31		1.14
	4D		1.48		1.35
n=5	5A	1.94(8)	2.06	1.73(9)	1.87
	5B		1.95		1.86
	5C		1.82		1.69
	5D		2.09		1.88
n=6	6A	1.97(8)	2.13	1.77(9)	1.90
	6B		2.16		1.99
	6C		2.03		1.76
	6D		2.18		1.89

[a] Numbers in parentheses represent the uncertainty in the last digit

3.2.1 MNi(CO)$_2^-$ (M = Sc, Y)

In Fig. 3, the lowest-lying isomer (labeled as 2A) of ScNi(CO)$_2^-$ is a C_1 structure with a ^{1}A ground state, in which two types of coordination configurations (i.e., side-on-bonded and terminal) are simultaneously involved and the terminal CO is bonded to the Ni atom. The second isomer (2B) has two side-on-bonded CO molecules and lies higher in energy above 2A by 0.06 eV. The 2C isomer (+0.30 eV) has side-on-bonded and bridging carbonyls. The 2D isomer (+1.20 eV) consists of one bridging carbonyl and one carbonyl terminally bonded to the Sc atom. As listed in Table 1, the calculated VDE of 2A (1.59 eV) is consistent with the experiment value of 1.76 ± 0.09 eV. The agreement of the calculated ADE value with the experiment value is also obtained for the 2A isomer (Table 1). The calculated VDEs and ADEs of isomers 2B–2D are much lower than the experimental values. It thus appears that the 2B–2D isomers

Table 2 Comparison of experimental VDE and ADE values to the calculated ones of the four lowest-energy isomers for $YNi(CO)_n^-$ ($n=2$–6)

Cluster	Isomer	VDE (eV)		ADE (eV)	
		Exp.[a]	Calc.	Exp.[a]	Calc.
$n=2$	2-I	1.70(9)	1.57	1.54(10)	1.41
	2-II		1.28		1.23
	2-III		1.20		1.17
	2-IV		0.93		0.84
$n=3$	3-I	1.89(8)	1.62	1.69(9)	1.50
	3-II		1.10		1.03
	3-III		1.24		1.10
	3-IV		1.22		1.09
$n=4$	4-I	1.96(8)	1.72	1.72(9)	1.57
	4-II		1.60		1.52
	4-III		1.51		1.38
	4-IV		1.14		1.05
$n=5$	5-I	2.12(7)	2.00	1.73(9)	1.79
	5-II		1.89		1.82
	5-III		1.72		1.61
	5-IV		1.93		1.76
$n=6$	6-I	2.26(6)	2.04	1.77(9)	1.82
	6-II		2.09		1.83
	6-III		2.02		1.89
	6-IV		1.95		1.78

[a] Numbers in parentheses represent the uncertainty in the last digit

do not contribute to the experimental spectrum. It can be seen from Fig. 4 that the calculated results of $YNi(CO)_2^-$ are similar to those of $ScNi(CO)_2^-$. The computed VDE and ADE values of 2-I (1.57 and 1.41 eV) are in agreement with experiment values (1.70 ± 0.09 and 1.54 ± 0.10 eV) (Table 2). The structures 2-II–2-IV can be excluded from the experiment.

3.2.2 $MNi(CO)_3^-$ ($M=$ Sc, Y)

The lowest-energy isomer of $ScNi(CO)_3^-$ (3A) is revealed by a C_s structure with a $^1A'$ ground state and consists of three types of coordination configurations (i.e., side-on-bonded, bridging, and terminal), in which the terminal carbonyl is bonded to the Ni atom (Fig. 3). The second energetically lying isomer (3B, +0.49 eV) has two side-on-bonded carbonyls and one terminal carbonyl. In 3C, it has three bridging mode. The 3D isomer reveals three different coordination modes, in which the terminal carbonyl is bonded to the Sc atom. The calculated VDE and ADE values for the most stable structure 3A (1.65 and 1.55 eV) are consistent with the experimental values of 1.83 ± 0.08 and 1.68 ± 0.09 eV (Table 1). The isomers 3B–3D should be too high in energy to be probed in the experiment, and their calculated VDE and ADE values could not fit as well with the experiment as compared to those of 3A. Similar results were also obtained for $YNi(CO)_3^-$ (Fig. 4; Table 2).

3.2.3 $MNi(CO)_4^-$ ($M=$ Sc, Y)

For the $n=4$ cluster, the lowest-energy isomer of $ScNi(CO)_4^-$ (4A) is a C_s structure with a $^1A'$ ground state, which consists of one side-on-bonded carbonyl, one bridging carbonyl, and two terminal carbonyls. The 4A structure could be viewed as being derived from 3A by terminally bonding the fourth CO molecule to the Sc atom. The 4B isomer lies higher in energy by 0.40 eV and consists of three bridging carbonyls and one terminal carbonyl. The third isomer (4C, +0.46 eV) has a C_s structure with two side-on-bonded CO groups and two terminal carbonyls. The 4D isomer has one side-on-bonded, one bridging, and two terminal carbonyls, in which the two terminal carbonyls are bonded to the Ni atom, different from the 4A structure. The calculated VDE and ADE values of 4A (1.76 and 1.60 eV) agree best with the experimental values of 1.86 ± 0.08 and 1.70 ± 0.09 eV (Table 1). This suggests that the 4A isomer should be responsible for the $n=4$ spectrum. For $YNi(CO)_4^-$, the lowest-energy isomer is similar to that of $ScNi(CO)_4^-$. Energetics of isomers 4-I–4-IV of $YNi(CO)_4^-$ is slightly different from isomers 4B–4D of $ScNi(CO)_4^-$. As listed in Table 2, the calculated VDE and ADE values of 4-I (1.72 and 1.57 eV) are also consistent with the experimental values of 1.96 ± 0.08 and 1.72 ± 0.09 eV.

3.2.4 $MNi(CO)_5^-$ ($M=$ Sc, Y)

The lowest-energy isomer of $ScNi(CO)_5^-$ (5A) has one side-on-bonded carbonyl, one bridging carbonyl, and three terminal carbonyls, in which one terminal carbonyl is bonded to the Ni atom and another two terminal carbonyls are bonded to the Sc atom. Next energetically lying isomer (5B, +0.22 eV) has two bridging carbonyls, two terminal carbonyls and one side-on-bonded carbonyl. The 5C isomer has three bridging carbonyls and two terminal carbonyls, which lies 0.35 eV higher in energy than the 5A isomer. The 5D isomer (+0.86 eV) has one bridging carbonyl, three carbonyls terminally bonded to the Sc atom, and one carbonyl terminally bonded to the Ni atom. As illustrated in Fig. 4, the structures for the isomers of $YNi(CO)_5^-$ are similar to $ScNi(CO)_5^-$. The calculated VDE and ADE values of the lowest-energy isomers for $MNi(CO)_5^-$ ($M=$ Sc, Y) are consistent with the experimental values (Tables 1, 2). The energetically higher-lying isomers could not be readily formed under the present experimental conditions.

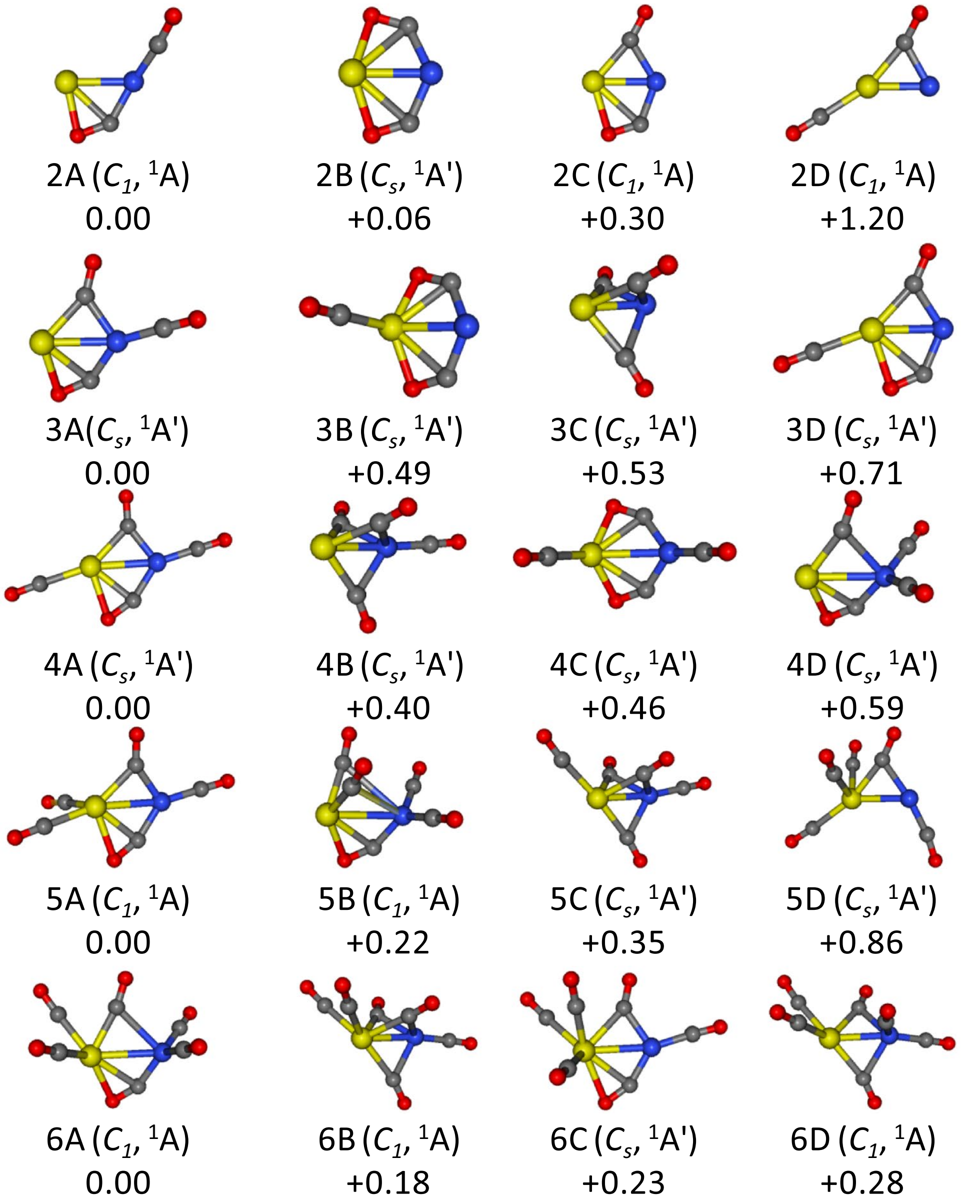

Fig. 3 Optimized structures of the four lowest-energy isomers for $\mathrm{ScNi(CO)}_n^-$ ($n=2$–6) (Sc, yellow; Ni, blue; C, gray; O, red). Relative energies are given in eV

3.2.5 $M\mathrm{Ni(CO)}_6^-$ ($M=\mathrm{Sc, Y}$)

For the $n=6$ cluster, the lowest-lying isomer of $\mathrm{ScNi(CO)}_6^-$ (6A) is indicated by a C_1 structure with a ^{1}A ground state, which consists of one side-on-bonded carbonyl, one bridging carbonyl, and four terminal carbonyls, in which two terminal carbonyls are bonded to the Sc atom and another two terminal carbonyls are bonded to the Ni atom. The 6B isomer (+ 0.18 eV) has three bridging carbonyls, and three terminal carbonyls, in which two terminal carbonyls are bonded to the Sc atom and another one terminal carbonyl is bonded to the Ni atom. The 6C isomer (+ 0.23 eV) has one side-on-bonded carbonyl, one bridging carbonyl, three carbonyls terminally bonded to the Sc atom, and one carbonyl terminally bonded to the Ni atom. The fourth isomer (6D) lies 0.28 eV above 6A and consists of two bridging carbonyls, two carbonyls terminally bonded to the Sc atom, and two carbonyls terminally bonded to the Ni atom. The isomers of $\mathrm{YNi(CO)}_6^-$ are analogous to those of $\mathrm{ScNi(CO)}_6^-$. The calculated VDE and ADE values of the lowest-energy isomers for $M\mathrm{Ni(CO)}_6^-$ ($M=$ Sc, Y) are in accord with the experimental values (Tables 1, 2). The other isomers should be too high in energy to be detected under the present experimental conditions.

4 Discussion

The agreement between the experimental and theoretical results allows for establishing the structural evolution of

Fig. 4 Optimized structures of the four lowest-energy isomers for $YNi(CO)_n^-$ ($n = 2–6$) (Y, yellow; Ni, blue; C, gray; O, red). Relative energies are given in eV

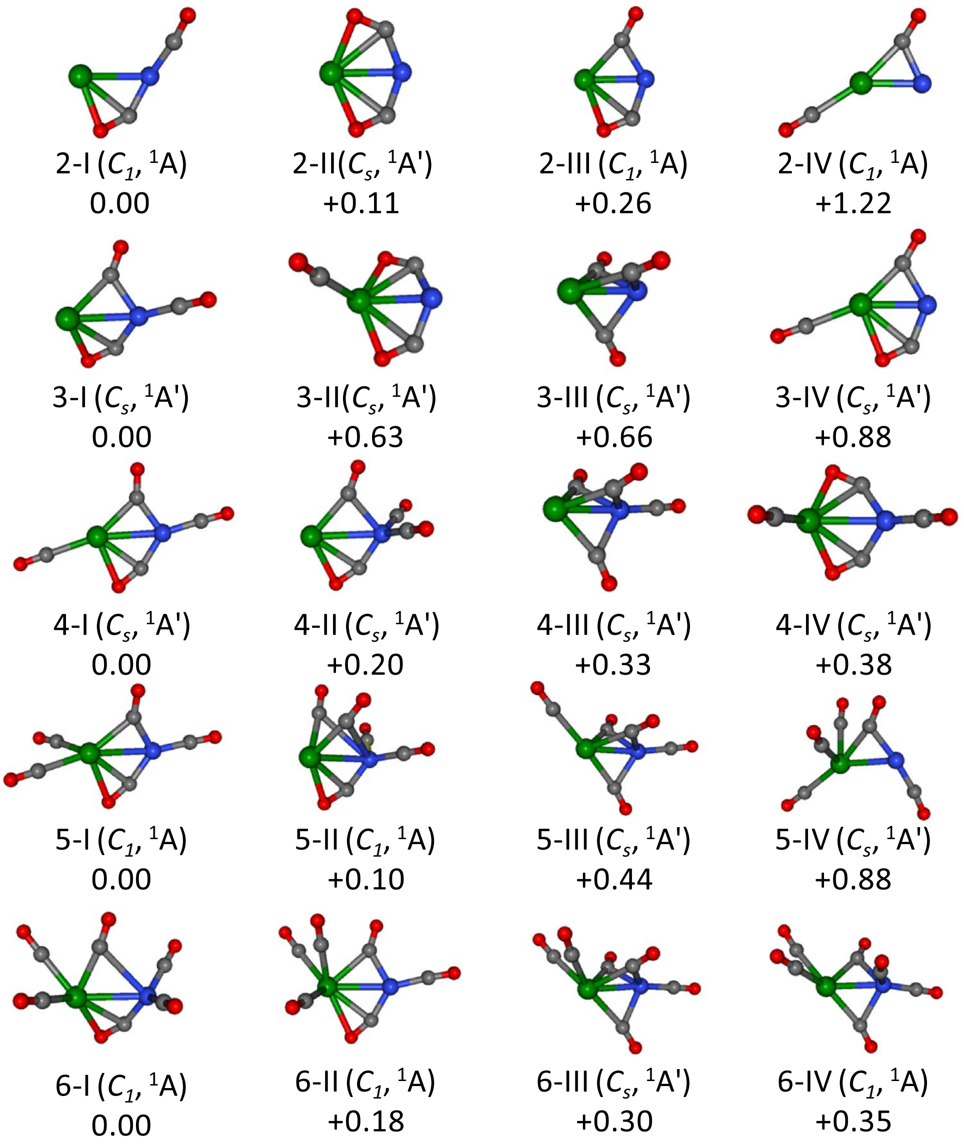

2-I (C_1, ^{1}A) 0.00
2-II(C_s, ^{1}A') +0.11
2-III (C_1, ^{1}A) +0.26
2-IV (C_1, ^{1}A) +1.22

3-I (C_s, ^{1}A') 0.00
3-II(C_s, ^{1}A') +0.63
3-III (C_s, ^{1}A') +0.66
3-IV (C_s, ^{1}A') +0.88

4-I (C_s, ^{1}A') 0.00
4-II (C_s, ^{1}A') +0.20
4-III (C_s, ^{1}A') +0.33
4-IV (C_s, ^{1}A') +0.38

5-I (C_1, ^{1}A) 0.00
5-II (C_1, ^{1}A) +0.10
5-III (C_s, ^{1}A') +0.44
5-IV (C_s, ^{1}A') +0.88

6-I (C_1, ^{1}A) 0.00
6-II (C_1, ^{1}A) +0.18
6-III (C_s, ^{1}A') +0.30
6-IV (C_1, ^{1}A) +0.35

$MNi(CO)_n^-$ ($M = Sc, Y$; $n = 2–6$). For these cluster anions, the VDE value increases with an increase of cluster size, which implies that the negative electron is stabilized upon the bonding of CO molecules. For $ScNi(CO)_2^-$, the 2A isomer has one side-on-bonded carbonyl and one terminal carbonyl. The 3A structure includes one side-on-bonded carbonyl, one bridging carbonyl, and one terminal carbonyl. The 4A isomer is derived from 3A by terminally bonding the fourth CO molecule to the Sc atom and the 5A structure is evolved from 4A by terminally bonding the fifth CO molecule to the Sc atom. The 6A isomer is derived from 5A by terminally bonding the sixth CO molecule to the Ni atom. In summary, two different kinds of CO bonding configurations (side-on-bonded and terminal carbonyls) are observed in the $n = 2$ cluster. The building block composed of three kinds of different CO modes (side-on-bonded, bridging, and terminal carbonyls) is favored at $n = 3$, the structure of which persists up to $n = 6$. The additional CO ligands are preferentially coordinated in the terminal mode to the Sc atom and then to the Ni atom in the larger clusters. Similar structural evolution was also obtained for $YNi(CO)_n^-$ ($n = 2–6$).

The molecular orbital pictures of the most stable isomers for $ScNi(CO)_n^-$ ($n = 2–6$) are shown in Fig. 5. The HOMO of 2A is π type bond feature, and the HOMO-1, HOMO-2, HOMO-3, and HOMO-4 are delocalized π orbitals mainly involving the metal–carbon unit. This suggests that the $ScNi(CO)_2^-$ cluster is stabilized by the π orbitals localized on the interaction of CO molecules with the ScNi binuclear cluster. Similar bonding features have also been obtained in the 3A–6A isomers (Fig. 5). The bonding mechanism of these clusters is analogous to the previous studies of $TiNi(CO)_n^-$ system, in which the C–O bonding is significantly weakened.

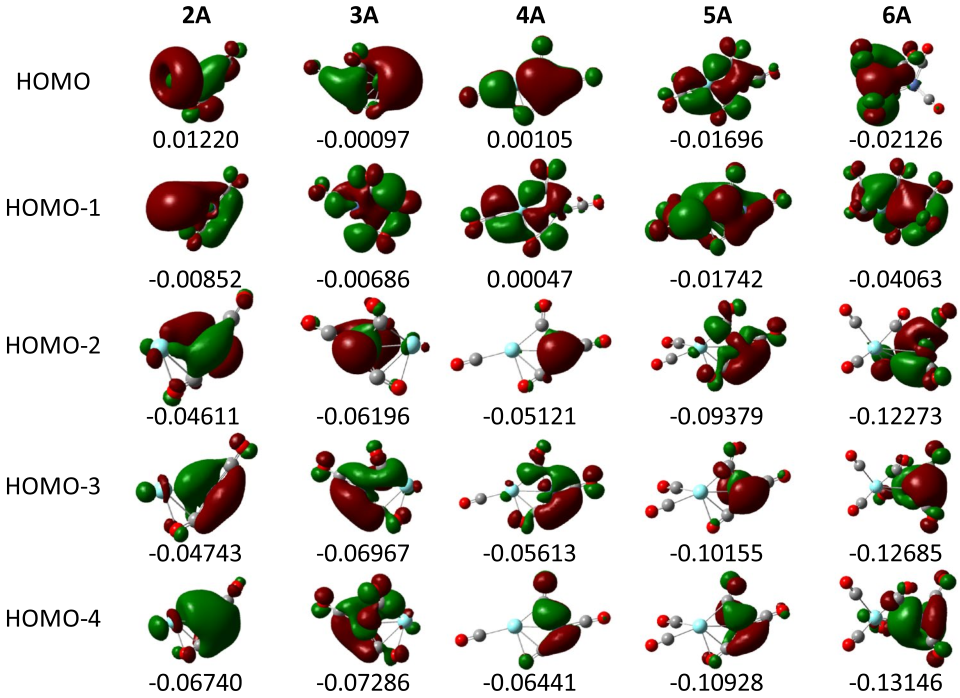

Fig. 5 Molecular orbital pictures of the most stable isomers for $ScNi(CO)_n^-$ ($n=2$–6) (2A–6A), showing the highest occupied molecular orbitals down to the fourth valence molecular orbital from the HOMO

It can be found from the above analysis that $MNi(CO)_2^-$ ($M=Sc$, Y) is capable of accommodating two different coordination modes (i.e., side-on-bonded and terminal modes), which is quite different from the homobinuclear carbonyl $Au_2(CO)_2^-$ with the involvement of two terminal CO ligands [34] and $Ti_2(CO)_2^-$ with the involvement of two side-on-bonded CO ligands [35]. The $MNi(CO)_3^-$ ($M=Sc$, Y) isomer has three different kinds of CO bonding fashions (side-on-bonded, bridging, and terminal carbonyls), which is similar to $TiNi(CO)_3^-$ [41], but different from other heterobinuclear metal–nickel carbonyls $MNi(CO)_3^-$ ($M=Mg$, Ca, Al, Cu) with the three carbonyls preferentially bonded to the nickel atom [38, 39]. The geometry of the $MNi(CO)_4^-$ ($M=Sc$, Y) isomer is different to the $CuFe(CO)_4^-$ and $PbFe(CO)_4^-$ clusters in which the carbonyls are bonded to the Ni or Fe atom [40, 52]. In contrast, the building block of three bridging CO molecules is favored in the $TiNi(CO)_n^-$ ($n=4$–6) clusters [41]. In $ScNi(CO)_2^-$, the C–O bond distance in the side-on-bonded and terminal mode was calculated to be about 1.24 and 1.16 Å, respectively, which is longer than that of the free CO molecule (1.13 Å). The CO stretching frequency of individual side-on-bonded and terminal carbonyl group in $ScNi(CO)_2^-$ was predicted to be 1528 and 1974 cm^{-1} (unscaled), respectively, pointing to the strong and weak C–O bond activation. Generally, the bridging and terminal bonding of CO on metal catalyst is a common feature. The $MNi(CO)_n^-$ ($M=Sc$, Y) systems reveal diverse patterns of metal–CO coordination covering from terminal to side-on-bonded mode, implying that the extent of C–O bond activation could be adjusted by tuning the cluster size. These findings would have important implications for understanding the CO activation and chemisorbed CO molecules on metal catalysts via the selection of different transition metals and metal compounds.

5 Conclusions

A series of heterobinuclear metal–nickel carbonyls $MNi(CO)_n^-$ ($M=Sc$, Y; $n=2$–6) have been generated via a laser vaporization supersonic cluster source and characterized by mass-selected photoelectron velocity-map imaging spectroscopy. Quantum chemical calculations have been carried out to elucidate the geometric and electronic structures and support the spectral assignments. Two CO bonding modes (side-on-bonded and terminal carbonyls) are involved in the $n=2$ cluster. The building block composed of three kinds of different CO modes (side-on-bonded, bridging, and terminal carbonyls) is favored at $n=3$, the structure of which persists up to $n=6$. The present findings provide important new insight into the structure and bonding mechanisms of CO molecules with heteronuclear transition metals, which would have important implications for understanding CO molecule activation and the chemisorbed CO molecules on alloy surfaces.

Acknowledgements This work was supported by the National Natural Science Foundation of China (Grants 21327901, 21503222, and 21673231), the Key Research Program (Grant KGZD-EW-T05), and the Strategic Priority Research Program (Grant XDB17010000) of the

Chinese Academy of Science. L. J. acknowledges the Hundred Talents Program of Chinese Academy of Sciences.

References

1. Heck RF (1974) Organotransition metal chemistry. Academic Press, New York
2. Huheey JE, Keiter EA, Keiter RL (1993) Inorganic chemistry principles of structure and reactivity harper collins. New York
3. Cotton FA, Wilkinson G, Murillo CA, Bochmann M (1999) Advanced inorganic chemistry 6th edn. Wiley, New York
4. Sunderlin LS, Wang D, Squires RR (1992) Metal (iron and nickel) carbonyl bond strengths in $Fe(CO)_n^-$ and $Ni(CO)_n$. J Am Chem Soc 114:2788–2796
5. Meyer F, Chen YM, Armentrout PB (1995) Sequential bond energies of $Cu(CO)_x^+$ and $Ag(CO)_x^+$ (x = 1–4). J Am Chem Soc 117:4071–4081
6. Spasov VA, Lee TH, Ervin KM (2000) Threshold collision-induced dissociation of anionic copper clusters and copper cluster monocarbonyls. J Chem Phys 112:1713–1720
7. Zhou MF, Andrews L (1999) Infrared spectra and density functional calculations of $Cu(CO)_{1-4}^+$,$Cu(CO)_{1-3}$, and $Cu(CO)_{1-3}^-$ in solid neon. J Chem Phys 111:4548–4557
8. Liang B, Zhou MF, Andrews L (2000) Reactions of laser-ablated Ni, Pd, and Pt atoms with carbon monoxide: matrix infrared spectra and density functional calculations on $M(CO)_n$ (n = 1–4), $M(CO)_n^-$ (n = 1–3), and $M(CO)_n^+$ (n = 1–2), (M = Ni, Pd, Pt). J Phys Chem A 104:3905–3914
9. Jiang L, Xu Q (2005) Reactions of gold atoms and small clusters with CO: infrared spectroscopic and theoretical characterization of Au_nCO (n = 1–5) and $Au_n(CO)_2$ (n = 1, 2) in solid argon. J Phys Chem A 109:1026–1032
10. Xu Q, Jiang L (2006) Oxidation of carbon monoxide on group 11 metal atoms: matrix-isolation infrared spectroscopic and density functional theory study. J Phys Chem A 110:2655–2662
11. Velasquez J, Duncan MA (2008) IR photodissociation spectroscopy of gas phase $Pt^+(CO)_n$ (n = 4–6). Chem Phys Lett 461:28–32
12. Velasquez J, Njegic B, Gordon MS, Duncan MA (2008) IR photodissociation spectroscopy and theory of $Au^+(CO)_n$ complexes: nonclassical carbonyls in the gas phase. J Phys Chem A 112:1907–1913
13. Ricks AM, Reed ZD, Duncan MA (2009) Seven-coordinate homoleptic metal carbonyls in the gas phase. J Am Chem Soc 131:9176–9177
14. Chi CX, Cui JM, Li ZH, Xing XP, Wang GJ, Zhou MF (2012) Infrared photodissociation spectra of mass selected homoleptic dinuclear iron carbonyl cluster anions in the gas phase. Chem Sci 3:1698–1706
15. Cui JM, Xing XP, Chi CX, Wang GJ, Liu ZP, Zhou MF (2012) Infrared photodissociation spectra of mass-selected homoleptic dinuclear palladium carbonyl cluster cations in the gas phase. Chin J Chem 30:2131–2137
16. Zhou X, Cui J, Li ZH, Wang GJ, Zhou MF (2012) Infrared photodissociation spectroscopic and theoretical study of homoleptic dinuclear chromium carbonyl cluster cations with a linear bridging carbonyl group. J Phys Chem A 116:12349–12356
17. Okabayashi T, Yamamoto T, Okabayashi EY, Tanimoto M (2011) Low-energy vibrations of the group 10 metal monocarbonyl MCO (M = Ni, Pd, and Pt): rotational spectroscopy and force field analysis. J Phys Chem A 115:1869–1877
18. Zhai HJ, Kiran B, Dai B, Li J, Wang LS Unique CO chemisorption properties of gold hexamer: $Au_6(CO)_n^-$ (n = 0–3). J Am Chem Soc 127:12098–12106
19. Stanzel J, Aziz EF, Neeb M (2007) Photoelectron spectroscopy on small anionic coppe – carbonyl clusters. Collect Czech Chem Commun 72:1–14
20. Zhai HJ, Pan LL, Dai B, Kiran B, Li J, Wang LS (2008) Chemisorption-induced structural changes and transition from chemisorption to physisorption in $Au_6(CO)_n^-$ (n = 4–9). J Phys Chem C 112:11920–11928
21. Pal R, Huang W, Wang YL, Hu HS, Bulusu S, Xiong XG, Li J, Wang LS, Zeng XC (2011) Chemisorption-induced 2D–3D–2D structural transitions in gold heptamer: $(CO)_nAu_7^-$ (n = 1–4). J Phys Chem Lett 2:2288–2293
22. Ignatyev IS, Schaefer HF, King RB, Brown ST (2000) Binuclear homoleptic nickel carbonyls: incorporation of Ni–Ni single, double, and triple bonds, $Ni_2(CO)_x$ (x = 5, 6, 7). J Am Chem Soc 122:1989–1994
23. Xie Y, Schaefer HF, King RB (2000) Binuclear homoleptic iron carbonyls: incorporation of formal iron–iron single, double, triple, and quadruple bonds, $Fe_2(CO)_x$ (x = 9, 8, 7, 6). J Am Chem Soc 122:8746–8761
24. Li Q, Liu Y, Xie Y, King RB, Schaefer HF (2001) Binuclear homoleptic copper carbonyls $Cu_2(CO)_x$ (x = 1–6): remarkable structures contrasting metal–metal multiple bonding with low-dimensional copper bonding manifolds. Inorg Chem 40:5842–5850
25. Zhou MF, Andrews L, Bauschlicher CW (2001) Spectroscopic and theoretical investigations of vibrational frequencies in binary unsaturated transition-metal carbonyl cations, neutrals, and anions. Chem Rev 101:1931–1962
26. Huber H, Kundig EP, Moskovits M, Ozin GA (1975) Binary copper carbonyls-synthesis and characterization of $Cu(CO)_3$, $Cu(CO)_2$, CuCO, and $Cu_2(CO)_6$. J Am Chem Soc 97:2097–2106
27. Huber H, Kundig EP, Ozin GA, Poe AJ (1975) Reactions of monatomic and diatomic manganese with carbon-monoxide-matrix infared spectroscopic evidence for pentacarbonylmanganese $MN(CO)_5$ and binuclear carbonyls $MN_2(CO)_n$ (where n = 1 or 2). J Am Chem Soc 97:308–314
28. Zhou MF, Chertihin GV, Andrews L (1998) Reactions of laser-ablated iron atoms with carbon monoxide: infrared spectra and density functional calculations of Fe_xCO, $Fe(CO)_x$, and $Fe(CO)_x^-$ (x = 1, 2, 3) in solid argon. J Chem Phys 109:10893–10904
29. Tremblay B, Manceron L, Gutsev GL, Andrews L, Partridge H (2002) Experimental and theoretical infrared spectra of Co_2CO. J Chem Phys 117:8479–8485
30. Jiang L, Xu Q (2006) Infrared spectroscopic and density functional theory studies on the CO dissociation by scandium and yttrium dimers. J Phys Chem A 110:5636–5641
31. Jiang L, Xu Q (2008) Theoretical study of the interaction of carbon monoxide with 3d metal dimers. J Chem Phys 128:124317
32. Cui JM, Zhou XJ, Wang GJ, Chi CX, Li ZH, Zhou MF (2014) Infrared photodissociation spectroscopy of mass-selected homoleptic cobalt carbonyl cluster cations in the gas phase. J Phys Chem A 118:2719–2727
33. Cui JM, Zhou XJ, Wang GJ, Chi CX, Liu ZH, Zhou MF (2013) Infrared photodissociation spectroscopy of mass selected homoleptic copper carbonyl cluster cations in the gas phase. J Phys Chem A 117:7810–7817
34. Wang YL, Zhai HJ, Xu L, Li J, Wang LS (2010) Vibrationally resolved photoelectron spectroscopy of di-gold carbonyl clusters $Au_2(CO)_n^-$ (n = 1–3): experiment and theory. J Phys Chem A 114:1247–1254
35. Zou JH, Xie H, Dai DX, Tang ZC, Jiang L (2016) Sequential bonding of CO molecules to a titanium dimer: a photoelectron velocity-map imaging spectroscopic and theoretical study of $Ti_2(CO)_n^-$ (n = 1–9). J Chem Phys 145:184302
36. Qu H, Kong FC, Wang GJ, Zhou MF (2016) Infrared photodissociation spectroscopic and theoretical study of heteronuclear

transition metal carbonyl cluster cations in the gas phase. J Phys Chem A 120:7287–7293

37. Qu H, Kong F, Wang GJ, Zhou MF (2017) Infrared photodissociation spectroscopy of heterodinuclear iron–zinc and cobalt–zinc carbonyl cation complexes. J Phys Chem A 121:1627–1632
38. Liu ZL, Xie H, Qin ZB, Fan HJ, Tang ZC (2014) Structural evolution of homoleptic heterodinuclear copper-nickel carbonyl anions revealed using photoelectron velocity-map Imaging. Inorg Chem 53:10909–10916
39. Xie H, Zou JH, Yuan QQ, Fan HJ, Tang ZC, Jiang L (2016) Photoelectron velocity-map imaging and theoretical studies of heteronuclear metal carbonyls $MNi(CO)_3^-$ (M = Mg, Ca, Al). J Chem Phys 144:124303
40. Zhang N, Luo M, Chi CX, Wang GJ, Cui JM, Zhou MF (2015) Infrared photodissociation spectroscopy of mass-selected heteronuclear iron-copper carbonyl cluster anions in the gas phase. J Phys Chem A 119:4142–4150
41. Zou JH, Xie H, Yuan QQ, Zhang JM, Dai DX, Fan HJ, Tang ZC, Jiang L (2017) Probing the CO bonding to heteronuclear group 4 metal-nickel clusters by photoelectron spectroscopy. Phys Chem Chem Phys 19:9790–9797
42. El-Bahy ZM (2013) Preparation and characterization of Pt-promoted NiY and CoY catalysts employed for 4-nitrophenol reduction. Appl Catal A-Gen 468:175–183
43. Yudasaka M, Sensui N, Takizawa M, Bandow S, Ichihashi T, Iijima S (1999) Formation of single-wall carbon nanotubes catalyzed by Ni separating from Y in laser ablation or in arc discharge using a C target containing a NiY catalyst. Chem Phys Lett 312:155–160
44. Podrebarac GG, Ng FTT, Rempel GL (1996) The effect of butadiene and reaction conditions on the dimerization of 1-butene over NiY zaolite. Appl Catal A-Gen 147:159–173
45. Zhou MF, Andrews L, Bauschlicher CW Jr (2001) Spectroscopic and theoretical investigations of vibrational frequencies in bibary unsaturated transition-metal carbonyl cations, neutrals, and anions. Chem Rev 101:1931–1962
46. Qin ZB, Wu X, Tang ZC (2013) A novel dual-channel time-of-flight mass spectrometer for photoelectron imaging spectroscopy. Rev Sci Instrum 84:066108
47. Frisch MJ, Trucks GW, Schlegel HB, Scuseria GE, Robb MA, Cheeseman JR, Scalmani G, Barone V, Mennucci B, Petersson GA, Nakatsuji H, Caricato M, Li X, Hratchian HP, Izmaylov AF, Bloino J, Zheng G, Sonnenberg JL, Hada M, Ehara M, Toyota K, Fukuda R, Hasegawa J, Ishida M, Nakajima T, Honda Y, Kitao O, Nakai H, Vreven T, Montgomery JA Jr, Peralta JE, Ogliaro F, Bearpark MJ, Heyd J, Brothers EN, Kudin KN, Staroverov VN, Kobayashi R, Normand J, Raghavachari K, Rendell AP, Burant JC, Iyengar SS, Tomasi J, Cossi M, Rega N, Millam NJ, Klene M, Knox JE, Cross JB, Bakken V, Adamo C, Jaramillo J, Gomperts R, Stratmann RE, Yazyev O, Austin AJ, Cammi R, Pomelli C, Ochterski JW, Martin RL, Morokuma K, Zakrzewski VG, Voth GA, Salvador P, Dannenberg JJ, Dapprich S, Daniels AD, Farkas O, Foresman JB, Ortiz JV, Cioslowski J, Fox DJ (2009) Gaussian 09, Gaussian, Inc.: Wallingford, CT
48. Becke AD (1993) Density-functional thermochemistry. III. The role of exact exchange. J Chem Phys 98:5648–5652
49. Brathwaite AD, Maner JA, Duncan MA (2014) Testing the limits of the 18-electron rule: the gas-phase carbonyls of Sc^+ and Y^+. Inorg Chem 53:1166–1169
50. Dunning TH (1989) Gaussian basis sets for use in correlated molecular calculations. I. The atoms boron through neon and hydrogen. J Chem Phys 90:1007–1023
51. Dolg M, Stoll H, Preuss H (1989) Energy adjusted abinitio pseudopotentials for the rare earth elements. J Chem Phys 90:1730–1734
52. Liu ZL, Zou JH, Qin ZB, Xie H, Fan HJ, Tang ZC (2016) Photoelectron velocity map imaging spectroscopy of lead tetracarbonyl–iron anion $PbFe(CO)_4^-$. J Phys Chem A 120:3533–3538